

Thermodynamic evidence for nematic superconductivity in $\text{Cu}_x\text{Bi}_2\text{Se}_3$

Shingo Yonezawa^{1*}, Kengo Tajiri¹, Suguru Nakata², Yuki Nagai³, Zhiwei Wang^{4,5}, Kouji Segawa^{4,6}, Yoichi Ando^{4,5} and Yoshiteru Maeno¹

In condensed matter physics, spontaneous symmetry breaking has been a key concept, and discoveries of new types of broken symmetries have greatly increased our understanding of matter^{1,2}. Recently, electronic nematicity, novel spontaneous rotational-symmetry breaking leading to an emergence of a special direction in electron liquids, has been attracting significant attention^{3–6}. Here, we show bulk thermodynamic evidence for nematic superconductivity, in which the nematicity emerges in the superconducting gap amplitude, in $\text{Cu}_x\text{Bi}_2\text{Se}_3$. Based on high-resolution calorimetry of single-crystalline samples under accurate two-axis control of the magnetic field direction, we discovered clear two-fold symmetry in the specific heat and in the upper critical field despite the trigonal symmetry of the lattice. Nematic superconductivity for this material should possess a unique topological nature associated with odd parity^{7–9}. Thus, our findings establish a new class of spontaneously symmetry-broken states of matter—namely, odd-parity nematic superconductivity.

The features of superconductivity are mostly governed by the superconducting (SC) gap Δ , or equivalently, by the SC wavefunction, which takes complex values with amplitude and phase degrees of freedom. Nematic superconductivity is characterized by spontaneous rotational-symmetry breaking (RSB) in the amplitude of the SC gap⁸ (Fig. 1a). Thus, once a nematic superconductor is cooled below its SC transition temperature T_c , RSB in various bulk properties is expected to emerge, while the RSB is absent in the normal (N) state⁹. We emphasize that nematic superconductors are distinct from known ‘unconventional’ superconductors such as p -wave or d -wave superconductors², in which spontaneous RSB occurs only in the phase factor of Δ , and thus phase-sensitive junction techniques are required to detect it¹⁰. Nematic superconductivity is also different from nematicity originating from the properties of normal-state conduction electrons recently found in various systems^{3–6}. Materials realization of nematic superconductivity has never been reported (see Supplementary Note 12 for details).

Among known superconductors, the copper-doped topological insulator $\text{Cu}_x\text{Bi}_2\text{Se}_3$ (ref. 11), consisting of triangular-lattice layers of Bi and Se with intercalated Cu between layers (Fig. 1b,c), is rather unique. In addition to the ordinary s -wave SC state Δ_1 , possible unconventional odd-parity SC states, labelled Δ_2 , Δ_3 , Δ_{4x} , and Δ_{4y} , originating from strong spin-orbit interactions and its multi-orbital nature have been proposed (Fig. 1d)^{7,12,13}. These odd-parity states can be also categorized as topological SC states, which are accompanied by stable surface states originating from the non-trivial topology of the SC wavefunction. Among these

states, the Δ_{4x} and Δ_{4y} states are predicted to be nematic SC states with a non-zero nematic order parameter⁸. Experimentally, the zero-bias conductance peak observed in the point-contact spectroscopy, indicating the existence of unusual surface states, evidences topological superconductivity¹⁴. On the other hand, a scanning tunnelling microscopy (STM) experiment on the ab -plane revealed s -wave-like tunnelling spectra¹⁵, which was later actually found to be inconsistent with the s -wave (Δ_1) scenario¹⁶. Rather, it was proposed that the STM spectra may be explained within the topological superconductivity scenario by taking into account the possible quasi-two-dimensional (Q2D) nature of the Fermi surface^{12,17}. More recently, by means of the nuclear-magnetic resonance (NMR), spin-rotational symmetry was revealed to be broken in the SC state¹⁸, suggesting realization of the Δ_{4x} or Δ_{4y} states.

In this Letter, based on the high-resolution specific-heat C measurements of single-crystalline $\text{Cu}_x\text{Bi}_2\text{Se}_3$ ($T_c \approx 3.2$ K) under accurate two-axis field-directional control using a vector magnet with a rotating stage¹⁹, we report thermodynamic evidence for spontaneous RSB in the SC gap amplitude for the first time among any known superconductors. We further obtained evidence for the Δ_{4y} state, with gap minima (or nodes) along one of the Bi–Bi bonding directions. Our results unambiguously show that $\text{Cu}_x\text{Bi}_2\text{Se}_3$ belongs to a new class of materials with odd-parity nematicity and topological superconductivity. We emphasize that the conclusion holds irrespectively of the dimensionality of the actual normal-state electronic structure (see Supplementary Note 9).

In Fig. 2a, we compare the dependence of C/T on the in-plane field angle ϕ for Sample #1 in the SC and N states. Here, as shown in Fig. 1c, we define the x -axis as one of the six equivalent Bi–Bi bond directions within the ab -plane, the y -axis as the direction perpendicular to x within the plane, and ϕ as the azimuthal angle of the field with respect to x . In addition, the z -axis is parallel to the c -axis and the angle θ is the polar angle with respect to z . Although C/T is independent of ϕ in the N state, $C(\phi)/T$ in the SC state unexpectedly exhibits clear two-fold oscillation. For the rhombohedral $R\bar{3}d$ crystal symmetry of $\text{Cu}_x\text{Bi}_2\text{Se}_3$, $C(\phi)/T$ should exhibit six-fold oscillation. Thus, the observed two-fold oscillation in $C(\phi)/T$ clearly breaks the rotational symmetry of the underlying lattice. The RSB is more easily recognized in the polar plot of $C(\phi)/T$ in Fig. 2b. A possible extrinsic origin for such RSB is field misalignment with respect to the ab -plane. To examine this possibility, we measured the dependence of C on the polar angle θ for various ϕ , presented as a surface colour plot in Fig. 2c (also see Supplementary Fig. 3). Evidently, $C(\theta)/T$ exhibits minima at

¹Department of Physics, Graduate School of Science, Kyoto University, Kyoto 606-8502, Japan. ²Faculty of Science, Kyoto University, Kyoto 606-8502, Japan. ³CCSE, Japan Atomic Energy Agency, Kashiwa, Chiba 277-0871, Japan. ⁴The Institute of Scientific and Industrial Research, Osaka University, Osaka 567-0047, Japan. ⁵Institute of Physics II, University of Cologne, Köln 50937, Germany. ⁶Department of Physics, Graduate School of Science, Kyoto Sangyo University, Kyoto 603-8555, Japan. *e-mail: yonezawa@scphys.kyoto-u.ac.jp

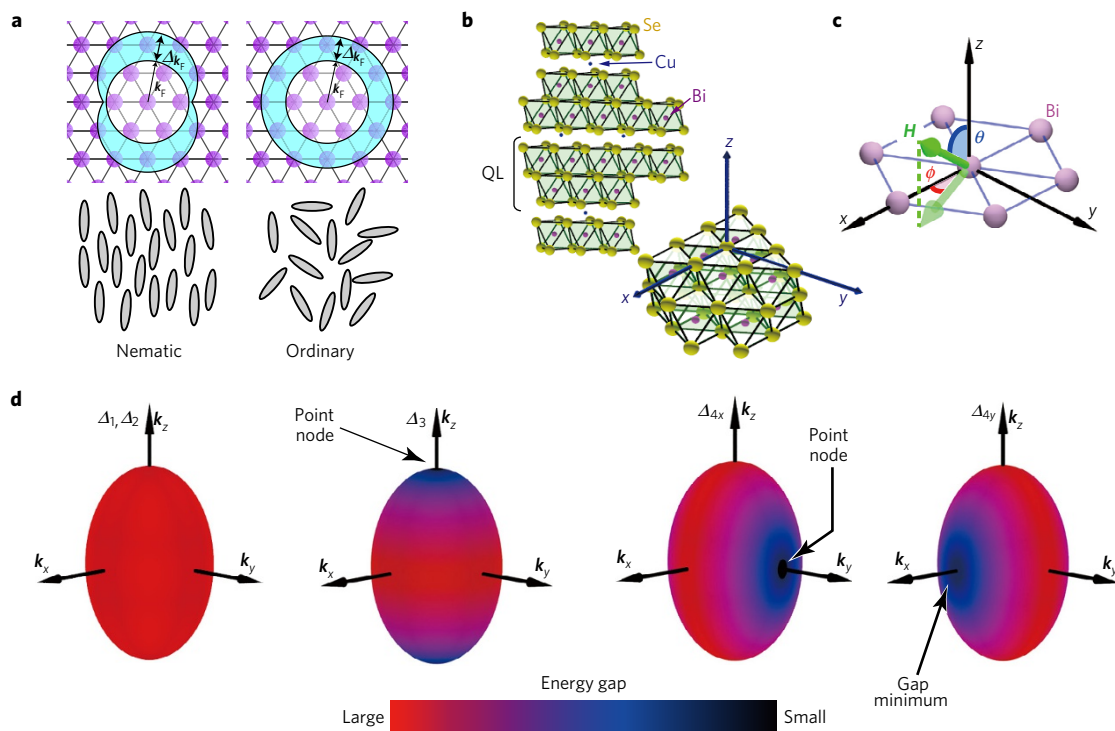


Figure 1 | Candidate material for nematic superconductivity: $\text{Cu}_x\text{Bi}_2\text{Se}_3$. **a**, Comparison of nematic and ordinary superconductivity in a hexagonal crystal system, with a nematic liquid-crystal phase and an ordinary liquid phase. The thickness of the blue region in the top panels illustrates the superconducting gap amplitude in the reciprocal space. The grey ovals in the bottom panels represent molecules in a liquid-crystal system. **b**, Crystal structure of $\text{Cu}_x\text{Bi}_2\text{Se}_3$ with $x \sim 0.3$. The structure of the quintuple layer (QL) is shown in the right bottom figure. **c**, Definitions of the axes and field angles with respect to the crystal structure. The purple spheres represent Bi atoms. **d**, Schematic description of SC gap structures Δ_1 , Δ_2 , Δ_3 , Δ_{4x} and Δ_{4y} proposed for $\text{Cu}_x\text{Bi}_2\text{Se}_3$ in refs 7,13. The ovals are Fermi surfaces, whose surface colour represents the gap magnitude, with black indicating $\Delta_k = 0$.

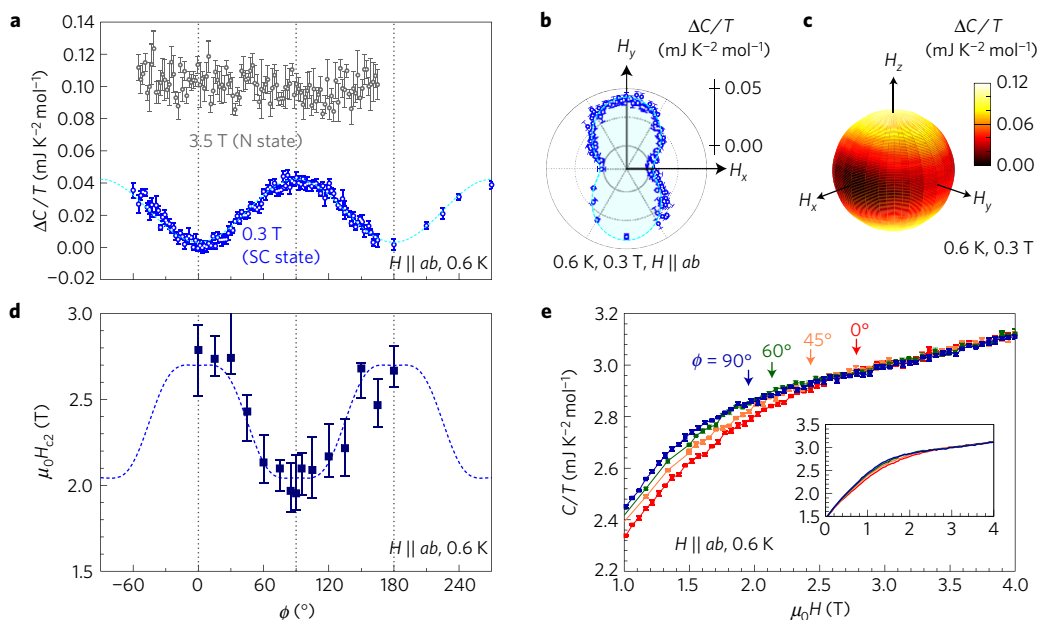


Figure 2 | Evidence for nematic superconductivity in $\text{Cu}_x\text{Bi}_2\text{Se}_3$. **a**, Oscillation of the specific heat at 0.6 K versus in-plane magnetic field angle in the SC state (0.3 T, blue points) compared to the data in the N state (3.5 T, grey points). Here, $\Delta C(\phi)/T$ is defined as $C(\phi)/T - C(\mathbf{H} \parallel \mathbf{x})/T$ and the data at 3.5 T are vertically shifted by $0.1 \text{ mJ K}^{-2} \text{ mol}^{-1}$. The broken curve is the fitting result with $\Delta C(\phi)/T = A_0 + A_2 \cos(2\phi)$. The data are obtained by averaging the specific-heat signal for typically 30–60 s, and the error bars indicate the standard deviation of the acquired raw data. **b**, Polar plot of $\Delta C(\phi)/T$ at 0.6 K and 0.3 T ($\mathbf{H} \parallel ab$), together with the fitting result. The polar angle of a data point in this 2D plot corresponds to the azimuthal field angle ϕ , and the distance from the origin indicates the magnitude of $\Delta C/T$. **c**, Colour map of $\Delta C(\theta, \phi)/T$ on a sphere in the H_x - H_y - H_z space, based on the θ -sweep data at 0.6 K and 0.3 T (see also Supplementary Fig. 3a). **d**, In-plane anisotropy of H_{c2} at 0.6 K. The definition of the error bars is explained in Supplementary Fig. 10. The broken curve presents the result of fitting with $H_{c2}(\phi) = H_0 + H_2 \cos(2\phi) + H_6 \cos(6\phi)$. **e**, In-plane magnetic-field dependence of the specific heat for various ϕ . The arrows mark H_{c2} . The inset presents data in the whole field range.

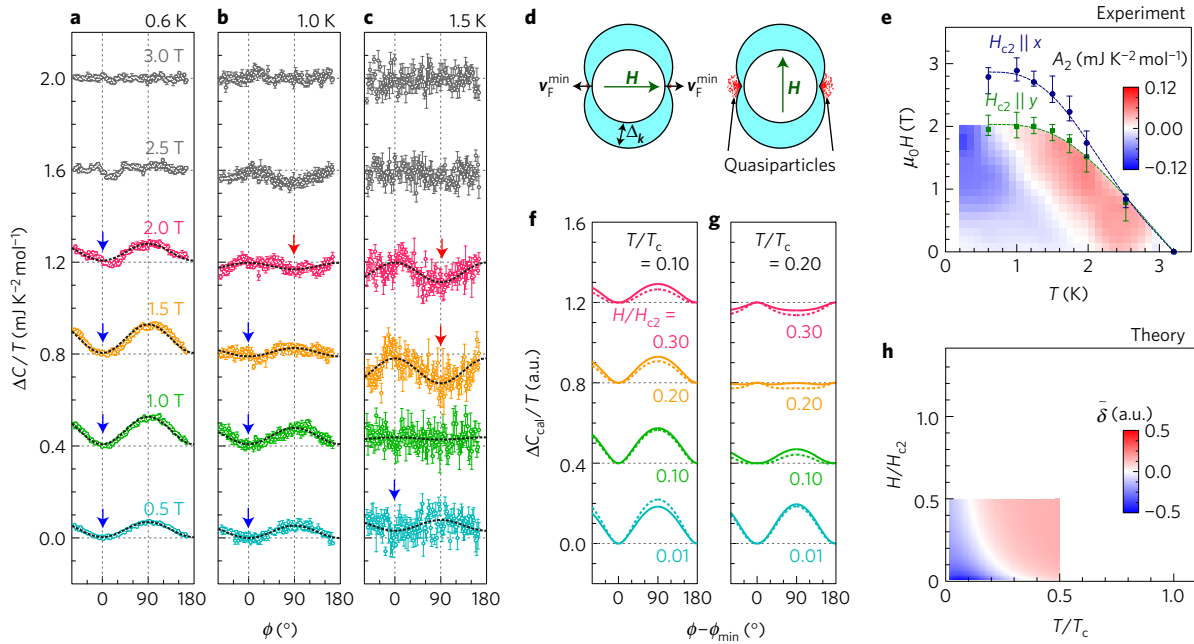


Figure 3 | Superconducting gap structure of $\text{Cu}_x\text{Bi}_2\text{Se}_3$. **a–c**, Experimental $\Delta C(\phi)/T$ data compared to fitting results with $A_0 + A_2 \cos(2\phi)$ (broken curves). Each curve is shifted vertically by $0.4 \text{ mJ K}^{-2} \text{ mol}^{-1}$. Notice that the sample is entirely in the N state at 3.0 T but is in the SC state near $\phi = 0^\circ$ at 2.5 T due to the H_{c2} anisotropy (see Fig. 2e). The vertical arrows indicate minimum positions in $\Delta C(\phi)/T$. For the definition of the error bars, see the caption of Fig. 2a. **d**, Schematics of the field-angle-dependent quasiparticle excitation (red dots) in the low-temperature and low-field limit. **e**, Colour map of A_2 within the SC phase. In the blue and red regions, $\Delta C(\phi)/T$ exhibits minima at $\phi = 0^\circ$ and 90° , respectively. The circles and squares indicate H_{c2} along x and y . The definition of the error bars in H_{c2} is explained in Supplementary Fig. 9. **f, g**, Calculated $\Delta C_{\text{cal}}(\phi)/T \equiv C_{\text{cal}}(\phi)/T - C_{\text{cal}}(\phi_{\text{min}})/T$ with offsets. Here, C_{cal} is the calculated specific heat and ϕ_{min} is the field direction where $\mathbf{H} \parallel \mathbf{v}_F^{\text{min}}$. The solid and broken curves are for point minima ($\Delta_{\text{min}}/\Delta_{\text{max}} = 0.1$) and for point nodes, respectively. **h**, Colour map of $\bar{\delta} \equiv C_{\text{cal}}(\phi_{\text{min}})/C_{\text{cal}}(\phi_{\text{min}} + 90^\circ) - 1$ for point-node gap. In the blue and red regions, $\Delta C_{\text{cal}}(\phi)/T$ exhibits a minimum and maximum at $\phi = \phi_{\text{min}}$, respectively.

$\theta = 90^\circ$ for any ϕ , excluding the possibility of field misalignment. In addition, the two-fold oscillation has been reproduced in several samples (Supplementary Fig. 7). Furthermore, one sample (#3) exhibits shifted and smaller oscillations, indicating the existence of multiple ‘nematic domains’, which manifest the spontaneous nature of the RSB (see Supplementary Note 7). Therefore, the rotational symmetry of the lattice is intrinsically and spontaneously broken in the SC state, evidencing nematic superconductivity in $\text{Cu}_x\text{Bi}_2\text{Se}_3$.

Next, we discuss the in-plane anisotropy of H_{c2} presented in Fig. 2d. In Fig. 2e, we present the field-strength dependence of C/T at 0.6 K for various in-plane field directions. Clearly, $C(H)/T$ curves again do not obey the expected six-fold rotational symmetry: the curves are substantially different between $\phi = 0^\circ$ and 60° . We here define H_{c2} as the onset of deviation from the linear field dependence in the N state (see Supplementary Note 10). The obtained $H_{c2}(\phi)$ (Fig. 2d) is clearly dominated by two-fold oscillation. Indeed, by fitting $H_{c2}(\phi)$ with $H_0 + H_2 \cos(2\phi) + H_6 \cos(6\phi)$, we obtain $\mu_0 H_0 = 2.37 \pm 0.03 \text{ T}$, $\mu_0 H_2 = 0.37 \pm 0.04 \text{ T}$, and $\mu_0 H_6 = -0.05 \pm 0.04 \text{ T}$. Interestingly, H_2 is as large as 16% of H_0 . This striking in-plane H_{c2} anisotropy not only supports the nematic SC state of $\text{Cu}_x\text{Bi}_2\text{Se}_3$, but also indicates the existence of a single nematic domain in this sample (see Supplementary Note 7).

As one can clearly see in Fig. 2, the observed in-plane field-angle dependences of C and H_{c2} are both dominated by the two-fold components. The large two-fold behaviour is probably due to the dominance of the two-fold component originating from the nematic SC order parameter over the ordinary component, such as the one originating from Fermi-surface anisotropy, as discussed in Supplementary Note 13.

Among the proposed SC states for $\text{Cu}_x\text{Bi}_2\text{Se}_3$, only the Δ_{4x} and Δ_{4y} states spontaneously break the in-plane rotational symmetry^{8,9}.

Thus, the observed bulk nematicity provides strong evidence for the two possible nematic states, the nodal Δ_{4x} state (with nodes along the \mathbf{k}_y -direction, protected by the mirror symmetry⁸) and the fully gapped Δ_{4y} state (with gap minima along the \mathbf{k}_x -direction; also see Supplementary Note 9) can be distinguished by the position of the gap minima or nodes. With this aim in mind, we investigate $C(\phi)/T$ of Sample #1, with a single nematic domain, in more detail. When the SC gap has minima (including nodes), C/T exhibits oscillatory behaviour as a function of field angle, because of the field-angle-dependent quasiparticle excitations originating from the gap anisotropy^{20,21}. At low-temperature and low-field conditions, C/T exhibits minima when the field is parallel to the Fermi velocity at a gap minimum $\mathbf{v}_F^{\text{min}}$, as shown in Fig. 3d. Furthermore, it has been predicted and observed that, in addition to the C/T oscillation originating from H_{c2} anisotropy, the C/T oscillations exhibit sign changes depending on the temperature and field conditions: for example, at intermediate temperatures, C/T exhibits maxima for $\mathbf{H} \parallel \mathbf{v}_F^{\text{min}}$ (refs 22,23). Thus, detailed experiments as well as comparison with theoretical calculations are required to conclude the gap structure.

Figure 3a–c represents the observed $C(\phi)/T$ curves in various conditions. Two-fold oscillation with a minimum at $\phi = 0^\circ$ ($\mathbf{H} \parallel \mathbf{x}$) is observed at 0.6 K in the SC state. However, at higher temperatures, the oscillation inverts sign above $\sim 1.5\text{--}2.0 \text{ T}$ at 1.0 K and $\sim 1.0 \text{ T}$ at 1.5 K, exhibiting a maximum at $\phi = 0^\circ$. The temperature and field dependence of the oscillation prefactor A_2 is summarized in Fig. 3e as a colour plot. A boundary between positive and negative A_2 exists within the SC phase. These observations are compared with theoretical calculations based on the Kramer–Pesch approximation in Fig. 3f,g. Here, we assume a gap structure with gap minima or point nodes along an in-plane direction $\phi = \phi_{\text{min}}$ on a spherical Fermi surface. The calculated $C(\phi)/T$ curves for both cases of

gap minima and nodes resemble the observed ones fairly well: they exhibit two-fold oscillation with a minimum for $\phi = \phi_{\min}$ at low temperatures and low fields, and reversed oscillation with a maximum for $\phi = \phi_{\min}$ at elevated temperatures. This oscillation inversion is due to contributions from the density of states at finite energies, as well as of quasiparticle scattering by vortices²². As shown in Fig. 3h, the phase-inversion line passes $T/T_c \sim 0.35$ near $H/H_{c2} = 0$ and $T/T_c \sim 0.15$ near $H/H_{c2} = 0.25$, again qualitatively similar to the observation (Fig. 3e).

From these agreements between experiment and theory, we conclude that the SC gap of $\text{Cu}_x\text{Bi}_2\text{Se}_3$ is Δ_{4y} , possessing gap minima or nodes lying along the k_x -direction. Although it is not straightforward to distinguish gap minima or nodes from our data alone, it is more natural to expect that the Δ_{4y} state is fully gapped to have gap minima, due to symmetry and energetic reasons⁸ (see Supplementary Note 9).

The odd-parity nematic SC state in $\text{Cu}_x\text{Bi}_2\text{Se}_3$ unveiled here is accompanied by a nematicity in the macroscopically coherent odd-parity wavefunction. In this respect, it is clearly distinct from any known nematic states realized in liquid crystals or in non-SC electrons. In the future, it would be interesting to investigate the unusual consequences of odd-parity nematic SC ordering, such as unusual quantization phenomena associated with topological defects or new collective modes arising from the nematic order parameter.

Note added in proof: We notice that a report on two-fold symmetric behaviour in resistivity of a related compound, $\text{Sr}_x\text{Bi}_2\text{Se}_3$, appeared on the arXiv server (arXiv:1603.04197; 14 March 2016) shortly after ours (arXiv:1602.08941; 29 February 2016). This work has been recently published²⁴.

Methods

Methods, including statements of data availability and any associated accession codes and references, are available in the [online version of this paper](#).

Received 28 March 2016; accepted 2 September 2016; published online 10 October 2016

References

- Anderson, P. W. *Basic Notions of Condensed Matter Physics* (Westview Press, 1997).
- Sigrist, M. & Ueda, K. Phenomenological theory of unconventional superconductivity. *Rev. Mod. Phys.* **63**, 239–311 (1991).
- Ando, Y., Segawa, K., Komiya, S. & Lavrov, A. N. Electrical resistivity anisotropy from self-organized one dimensionality in high-temperature superconductors. *Phys. Rev. Lett.* **88**, 137005 (2002).
- Borzi, R. A. *et al.* Formation of a nematic fluid at high fields in $\text{Sr}_3\text{Ru}_2\text{O}_7$. *Science* **315**, 214–217 (2007).
- Kasahara, S. *et al.* Electronic nematicity above the structural and superconducting transition in $\text{BaFe}_2(\text{As}_{1-x}\text{P}_x)_2$. *Nature* **486**, 382–385 (2012).
- Okazaki, R. *et al.* Rotational symmetry breaking in the hidden-order phase of URu_2Si_2 . *Science* **331**, 439–442 (2011).
- Fu, L. & Berg, E. Odd-parity topological superconductors: theory and application to $\text{Cu}_x\text{Bi}_2\text{Se}_3$. *Phys. Rev. Lett.* **105**, 097001 (2010).
- Fu, L. Odd-parity topological superconductor with nematic order: application to $\text{Cu}_x\text{Bi}_2\text{Se}_3$. *Phys. Rev. B* **90**, 100509(R) (2014).

- Nagai, Y., Nakamura, H. & Machida, M. Rotational isotropy breaking as proof for spin-polarized Cooper pairs in the topological superconductor $\text{Cu}_x\text{Bi}_2\text{Se}_3$. *Phys. Rev. B* **86**, 094507 (2012).
- Tsuei, C. C. & Kirtley, J. R. Pairing symmetry in cuprate superconductors. *Rev. Mod. Phys.* **72**, 969–1016 (2000).
- Hor, Y. S. *et al.* Superconductivity in $\text{Cu}_x\text{Bi}_2\text{Se}_3$ and its implications for pairing in the undoped topological insulator. *Phys. Rev. Lett.* **104**, 057001 (2010).
- Ando, Y. & Fu, L. Topological crystalline insulators and topological superconductors: from concepts to materials. *Annu. Rev. Condens. Matter Phys.* **6**, 361–381 (2015).
- Sasaki, S. & Mizushima, T. Superconducting doped topological materials. *Physica C* **514**, 206–217 (2015).
- Sasaki, S. *et al.* Topological superconductivity in $\text{Cu}_x\text{Bi}_2\text{Se}_3$. *Phys. Rev. Lett.* **107**, 217001 (2011).
- Levy, N. *et al.* Experimental evidence for s-wave pairing symmetry in superconducting $\text{Cu}_x\text{Bi}_2\text{Se}_3$ single crystals using a scanning tunneling microscope. *Phys. Rev. Lett.* **110**, 117001 (2013).
- Mizushima, T., Yamakage, A., Sato, M. & Tanaka, Y. Dirac-fermion-induced parity mixing in superconducting topological insulators. *Phys. Rev. B* **90**, 184516 (2014).
- Lahoud, E. *et al.* Evolution of the Fermi surface of a doped topological insulator with carrier concentration. *Phys. Rev. B* **88**, 195107 (2013).
- Matano, K. *et al.* Spin-rotation symmetry breaking in the superconducting state of $\text{Cu}_x\text{Bi}_2\text{Se}_3$. *Nat. Phys.* **12**, 852–854 (2016).
- Deguchi, K., Ishiguro, T. & Maeno, Y. Field-orientation dependent heat capacity measurements at low temperatures with a vector magnet system. *Rev. Sci. Instrum.* **75**, 1188–1193 (2004).
- Vekhter, I., Hirschfeld, P. J., Carbotte, J. P. & Nicol, E. J. Anisotropic thermodynamics of d-wave superconductors in the vortex state. *Phys. Rev. B* **59**, R9023–R9026 (1999).
- Sakakibara, T. *et al.* Nodal structures of heavy fermion superconductors probed by the specific-heat measurements in magnetic fields. *J. Phys. Soc. Jpn* **76**, 051004 (2007).
- Vorontsov, A. & Vekhter, I. Nodal structure of quasi-two-dimensional superconductors probed by a magnetic field. *Phys. Rev. Lett.* **96**, 237001 (2006).
- An, K. *et al.* Sign reversal of field-angle resolved heat capacity oscillations in a heavy fermion superconductor CeCoIn_5 and $d_{x^2-y^2}$ pairing symmetry. *Phys. Rev. Lett.* **104**, 037002 (2010).
- Pan, F. *et al.* Rotational symmetry breaking in the topological superconductor $\text{Sr}_x\text{Bi}_2\text{Se}_3$ probed by upper-critical field experiments. *Sci. Rep.* **6**, 28632 (2016).

Acknowledgements

We acknowledge T. Watashige, S. Kasahara and Y. Kasahara for their technical assistance and L. Fu, M. Ueda, Y. Yanase, J. Yamamoto, Y. Matsuda, A. Yamakage, Y. Tanaka and T. Mizushima, for fruitful discussions. This work was supported by JSPS Grant-in-Aids for Scientific Research on Innovative Areas on ‘Topological Quantum Phenomena’ (KAKENHI JP22103002, JP22103004) and ‘Topological Materials Science’ (KAKENHI JP15H05852, JP15H05853, JP16H00995), JSPS Grant-in-Aids KAKENHI JP26287078, JP26800197, and DFG CRC1238 ‘Control and Dynamics of Quantum Materials’, Project A04.

Author contributions

This study was designed by S.Y., Y.A. and Y.M.; K.T. and S.Y. performed specific-heat measurements and analyses, with assistance from S.N. and guidance from Y.M.; Z.W., K.S. and Y.A. grew single-crystalline samples and characterized them. Y.N. performed theoretical calculations. The manuscript was prepared mainly by S.Y. and K.T., based on discussions among all authors.

Additional information

Supplementary information is available in the [online version of the paper](#). Reprints and permissions information is available online at www.nature.com/reprints. Correspondence and requests for materials should be addressed to S.Y.

Competing financial interests

The authors declare no competing financial interests.

Methods

Sample preparation and characterization. Single crystals of Bi_2Se_3 were grown by a conventional melt-growth method. Single-crystal samples of $\text{Cu}_x\text{Bi}_2\text{Se}_3$ were then obtained by intercalating Cu to single crystals of Bi_2Se_3 by means of an electrochemical technique²⁵. The value of the Cu content x was determined by the total charge flow during the intercalation process, as well as by the mass change between before and after the intercalation. The crystal axis directions were determined from Laue photos before the intercalation. The onset T_c was checked by using a superconducting quantum interference device (SQUID) magnetometer (MPMS, Quantum Design). After this process, the samples were stored in vacuum until they were mounted to the calorimeter. In the present study, we used three samples, which are labelled Samples #1, #2 and #3. All samples are single crystals of rectangular shapes with $x \approx 0.3$. The characteristics of each sample are listed in Supplementary Table 1.

Specific-heat measurement. We used a ^3He - ^4He dilution refrigerator (Kelvinox 25, Oxford Instruments) to cool down the samples. We performed specific-heat measurement in the temperature range $0.09\text{ K} \leq T \leq 4\text{ K}$. We constructed a custom-made high-resolution calorimeter²⁶, shown in Supplementary Fig. 1a. In our calorimeter, a sample was sandwiched between a thermometer and a heater, both of which were made using RuO_2 chip resistors. We mounted a sample inside a glove box with an Ar atmosphere. We measured the specific heat by using the a.c. method²⁷: we applied an a.c. current to the heater using a current source (6221, Keithley Instruments), and measured the resultant temperature modulation amplitude T_{ac} and the phase shift ϕ_{ac} using lock-in amplifiers (SR830, Stanford Research Systems). The offset sample temperature T was also recorded by another lock-in amplifier. An excitation current to the thermometer was applied using another current source. For most of the data, the raw heat capacity C_{raw} was then obtained as $C_{raw} = [P/(2\omega_H T_{ac})] \sin \phi_{ac}$, where P is the a.c. heat flow produced by the heater and ω_H is the frequency of the heater current. Multiplication by the factor $\sin \phi_{ac}$ allows for more accurate evaluation of the heat capacity, even for smaller frequencies²⁸. Notice that the frequency of the temperature oscillation is two times higher than ω_H . We typically used $\omega_H = 1.3\text{ Hz}$ and $T_{ac}/T \sim 1.5\text{--}2.0\%$ for measurements. For the temperature dependence of C/T below 0.6 K and at zero field (Supplementary Fig. 2), we evaluated C_{raw} by another method to improve the accuracy: we measured the ω_H dependence of T_{ac} and fitted $T_{ac}(\omega_H)$ with the function $T_{ac}(\omega_H) = [P/(4\omega_H C_{raw})][1 + (2\omega_H \tau_1)^2 + (2\omega_H \tau_2)^2]^{-1/2}$ to obtain C_{raw} , where τ_1 and τ_2 are the external and internal relaxation times, respectively. The heat capacity of the sample stage (addenda) was measured separately by using a piece of pure silver as a reference sample, and subtracted from the total heat capacity to extract the sample contribution. The addenda contribution is typically 10–20% of the total heat capacity. We confirmed that the addenda does not produce detectable changes in either the θ or ϕ dependences.

Magnetic-field control. We applied the magnetic field using a vector-magnet system¹⁹, which consists of two orthogonal superconducting solenoids (pointing in the vertical and horizontal directions, respectively) and a rotation stage, as schematically shown in Supplementary Fig. 1c. Within the laboratory frame, we can rotate the magnetic field both vertically, by changing the relative field strengths of the two orthogonal solenoids, and horizontally, by using the horizontal rotation stage. For the vertical rotation, the magnetic field of the solenoids can be controlled with a resolution of 0.1 mT , which results in an angular resolution of 0.006° at 1 T

and 0.06° at 0.1 T . The horizontal rotator has an angular resolution of 0.001° , with negligible backlash. Thus, this system allows for a precise two-axis control of the field direction. The directions of the crystalline axes with respect to the laboratory frame are determined by making use of the anisotropy in H_{c2} . Once the directions of the crystalline axes are determined, we can rotate the magnetic field within the sample frame with the aid of our automation software. All field angle values presented in this Letter are defined in the sample frame. The precision and accuracy of the field alignment are approximately 1° . Notice that this is worse than those achieved for more anisotropic superconductors such as Sr_2RuO_4 (ref. 26), because of the relatively small out-of-plane H_{c2} anisotropy of $\text{Cu}_x\text{Bi}_2\text{Se}_3$ (see Supplementary Note 11). Nevertheless, this small anisotropy of $\text{Cu}_x\text{Bi}_2\text{Se}_3$ in turn makes the misalignment effect rather small, as explained in Supplementary Note 3.

Theoretical calculation. The field-angle-dependent heat capacity is calculated on the basis of the Kramer–Pesch approximation, which is appropriate in a low-magnetic-field region²⁹. By using the quasiclassical framework, a Dirac Bogoliubov–de Gennes (BdG) Hamiltonian which describes a topological superconductivity with point nodes derived from the first-principle calculations is reduced to a BdG Hamiltonian for spin-triplet p -wave superconductivity. The corresponding \mathbf{d} -vector is $\mathbf{d}(\mathbf{k}_F) = (v_{Fz} \sin \phi_N, -v_{Fz} \cos \phi_N, v_{Fy} \cos \phi_N - v_{Fx} \sin \phi_N)$. For this state, point nodes are located in the ϕ_N -direction on the ab -plane³⁰. Here, we consider a three-dimensional spherical Fermi surface. In the case of a fully gapped order parameter with gap minima, we consider the gap $|\Delta(\mathbf{k})| = |\mathbf{d}(\mathbf{k}_F)|(1-r) + |\mathbf{d}|_{\max} r$, where $|\mathbf{d}|_{\max}$ is the maximal value of $|\mathbf{d}(\mathbf{k}_F)|$ and r ($0 < r < 1$) corresponds to the ratio between the minimal and maximal values of $|\Delta(\mathbf{k}_F)|$. We also performed calculations for a Q2D Fermi surface. We used a Q2D tight-binding model for the normal-state electronic band¹⁷ and assumed a point-nodal gap³¹, as schematically shown in the inset of Supplementary Fig. 6c.

Data availability. Data supporting the plots within this paper and other findings of this study are available from the corresponding author upon reasonable request.

References

- Kriener, M., Segawa, K., Ren, Z., Sasaki, S. & Ando, Y. Bulk superconducting phase with a full energy gap in the doped topological insulator $\text{Cu}_x\text{Bi}_2\text{Se}_3$. *Phys. Rev. Lett.* **106**, 127004 (2011).
- Yonezawa, S., Kajikawa, T. & Maeno, Y. First-order superconducting transition of Sr_2RuO_4 . *Phys. Rev. Lett.* **110**, 077003 (2013).
- Sullivan, P. F. & Seidel, G. Steady-state, ac-temperature calorimetry. *Phys. Rev.* **173**, 679–685 (1968).
- Velichkov, I. On the problem of thermal link resistances in a.c. calorimetry. *Cryogenics* **32**, 285–290 (1992).
- Nagai, Y., Nakamura, H. & Machida, M. Superconducting gap function in the organic superconductor $(\text{TMTSF})_2\text{ClO}_4$ with anion ordering: First-principles calculations and quasiclassical analysis for angle-resolved heat capacity. *Phys. Rev. B* **83**, 104523 (2011).
- Nagai, Y. Field-angle-dependent low-energy excitations around a vortex in the superconducting topological insulator $\text{Cu}_x\text{Bi}_2\text{Se}_3$. *J. Phys. Soc. Jpn* **83**, 063705 (2014).
- Hashimoto, T., Yada, K., Yamakage, A., Sato, M. & Tanaka, Y. Effect of Fermi surface evolution on superconducting gap in superconducting topological insulator. *Supercond. Sci. Technol.* **27**, 104002 (2014).